Numerical Simulations for Electro-Osmotic Blood Flow of Magnetic Sutterby Nanofluid with Modified Darcy's Law

NOURREDDINE SFINA[1], M. G. IBRAHIM[2*]
[1]College of Sciences and Arts in Mahayel Asir, Department of Physics,
King Khalid University,
Abha,
SAUDI ARABIA

[2]Basic and Applied Science Department,
International Academy for Engineering and Media Science,
EGYPT

*Corresponding Author

Abstract: -   Owing to the considerable significance of the combination of modified law of Darcy and electric fields in biomedicine applications like drug design, and pumping of blood in heart and lung devices; so, numerical and physiological analysis on electro-osmotic peristaltic pumping of magnetic Sutterby Nanofluid is considered. Such a fluid model has not been studied before in peristaltic. The applied system of differential equations is obtained by using controls of low Reynolds number and long wavelength. Simulations for a given system are counted using two high-quality techniques, the Finite difference technique (FDM) and the Generalized Differential transform method (Generalized DTM). Vital physical parameters effects on the profiles of velocity, temperature, and Nanoparticle concentration have schemed in two different states of Sutterby fluid, the first is dilatant fluid at $\beta < 0$ and Pseudo plastic fluid at $\beta > 0$. A comparison between the prior results computed by FDM and Generalized-DTM and literature results are given in nearest published results have been made, and found to be excellent. The discussion puts onward a crucial observation, that the velocity of blood flow can be organized by adaptable magnetic field strength. A drug delivery system is considered one of the significant applications of such a fluid model.

1 Introduction

Nowadays, non-Newtonian fluid has a vital role in many engineering processes and physiological applications as the modelers, physicians, engineers, and academic's interested. Sutterby fluid is a sub-class of non-Newtonian fluid and it's considered a framework that demonstrates dilute polymer solutions and is utilized to investigate the properties of rheological of numerous materials, [1]. In the flow of the boundary layer, The study, [2], scrutinized the mixed convection of heat transfer in an eccentric annulus. In peristaltic flow, [3], addressed the effects of chemical reactions on Sutterby fluid in the presence of exploration and transportation properties. The authors in, [4], [5], introduce a new mechanism of the peristaltic model of non-Newtonian fluid with radiative heat transfer. All published research in this area has emphasized the importance of Sutterby fluid flow, [1], [2], [3], [4], [5].

Huge popularity in the 1990s has been ongoing towards a new area called Electro-osmotic flow because of its vital paramount role in medicine and Biomedicine. Strong thumps utilized in electroporation are used to advance the insertion of DNA into cell nuclei and drugs into tumors, [7]. The study, [8], studied a Bio-rheological fluid in a uniform channel in the presence of the influence of electroosmosis. The study, [9], elucidates a Bingham fluid flow under electroosmosis effects in a symmetric channel, they found that the fluid velocity distribution and temperature are increasing functions in the electroosmosis parameter. The study, [10],

addressed the influence of the electro-magneto-hydrodynamic fluid flow in the presence of wall slip effects. Many vital applications of electroosmosis can be found in, [11], [12], [13], [14], [15], [16], [17], [18], [19], [20].

The main idea of Dray's law started in the eighteenth century exactly 1865 by, [21], [22], Darcy's law or Darcy's equation is a constitutive equation derived from a physical phenomenon that designates the fluid flow concludes a porous medium. Henry Darcy's Law in the eighteenth century was constructed on the results of experiments on the flow of water concluded a sand medium. In addition, they form the scientific basis for fluid permeability utilized in earth sciences, expressly in hydrogeology. Darcy's law has many applications, one of them is the flow of water in an aquifer. Conservation of mass equation due to Darcy's law in the case of equals the groundwater flow equation, which is one of the important associations in hydrogeology. In addition, Darcy's Law is utilized to designate the flows of oil, water, and gas concluded oil. The study, [23], studied the entropy generation effects of the MHD flow of Jeffery fluid in the presence of Darcy. The study, [24], scrutinized the improved Darcy's law in peristaltic transport. There are many applicants of Darcy law in the nearest published papers, for more information, [25].

The generalized method of differential transform method is a highly accurate technique introduced in the last years of the last century by, [26]. In fluid mechanics, many investigations use the algorithms of generalized DTM to get a highly verified result for fluid models, [27], [28], [29], [30], [31], [32], [33], [34], [35]. To get the numerical and graphical results, FDM and generalized DTM are used. The numerical results show that there is a good agreement between the prior results and existing published results by results by, [4]. By the above-mentioned studies, the main paper aims to introduce the electro-osmotic effects on MHD Sutterby in the case of modified Darcy's law. Three cases in our study have been mentioned concerning the characteristics of the proposed model. 1st order chemical reactions and thermal radiation influences, appear in our modeling discussion. The effects of numerous non-dimensionless parameters of concern are obtainable through graphs and tables. Biomedicine interpretations of the obtainable results are thoroughly debated, and the vital conclusions are then abstracted.

2 Model Form

The electroosmosis and generalized Darcy law are elucidated on peristaltic pumps of Sutterby fluid, in a channel width $d_1 + d_2$ concluded. The propagating wave velocity is denoted by (c) and magnetic (B_0) field to the walls of channel $Y - axis$, (Figure 1).
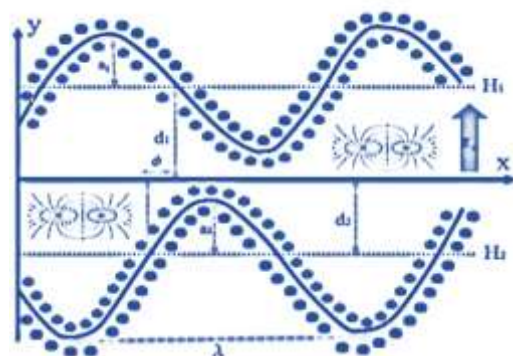

Fig. 1: Electroosmosis physical fluid model

$$Y = H_1(X,t) = d_1 + a_1 \cos\left[\frac{2\pi}{\lambda}(X - ct)\right]$$
Upper wall $\qquad(1)$

$$Y = H_2(X,t) = -d_2 - b_1 \cos\left[\frac{2\pi}{\lambda}(X - ct) + \phi\right]$$ Lower wall $\qquad(2)$

Here, phase (ϕ) difference, the wave (λ) length, the amplitudes (a_1, a_2) waves, width $(d_1 + d_2)$ mean, the range of ϕ between (0), and (π), all of these contents are satisfying the following, [25]:

$$a_1^2 + a_2^2 + 2a_1 a_2 cos\phi \leq (d_1 + d_2)^2 \qquad(3)$$

Sutterby (τ) fluid can be expressed by, [4]

$$\tau = \frac{\mu}{2}\left[\frac{sinh^{-1}(D\dot{\xi})}{D\dot{\xi}}\right]^m A_1, \qquad(4)$$

Rivlin Erickson $\dot{\xi} = \sqrt{\frac{trac\, A_1^2}{2}}$ tensor, $A_1 = grad(V) + (grad(V))^t$, viscosity (μ), material. So, the fluid model is proposed as follows, [3], [4], [5], [6], [32], [33], [34]:

$$\frac{\partial \bar{U}}{\partial \bar{X}} + \frac{\partial \bar{V}}{\partial \bar{Y}} = 0, \qquad(5)$$

The momentum equation:
$$\rho\left[\frac{\partial \bar{U}}{\partial t} + \bar{U}\frac{\partial \bar{U}}{\partial \bar{X}} + \bar{V}\frac{\partial \bar{U}}{\partial \bar{Y}}\right] = -\frac{\partial \bar{P}}{\partial \bar{X}} + \frac{\partial \bar{\tau}_{XX}}{\partial \bar{X}} + \frac{\partial \bar{\tau}_{XY}}{\partial \bar{Y}} + \bar{\rho}_e E_X + \bar{R}_x + (1 - \bar{C}_0)\rho_f g\alpha^*(\bar{T} - T_0) + (\rho_p - \rho_f)g\beta^*(\bar{C} - C_0), \qquad(6)$$

$$\rho \left[\frac{\partial \bar{U}}{\partial t} + \bar{U}\frac{\partial \bar{U}}{\partial \bar{X}} + \bar{V}\frac{\partial \bar{U}}{\partial \bar{Y}}\right] = -\frac{\partial \bar{P}}{\partial \bar{Y}} + \frac{\partial \bar{\tau}_{YX}}{\partial \bar{X}} + \frac{\partial \bar{\tau}_{YY}}{\partial \bar{Y}} - \sigma B_0^2 \bar{V} + \bar{R}_y, \tag{7}$$

The heat equation

$$(\rho c)_f \left[\frac{\partial \bar{T}}{\partial t} + \bar{U}\frac{\partial \bar{T}}{\partial \bar{X}} + \bar{U}\frac{\partial \bar{T}}{\partial \bar{Y}}\right] = k\left(\frac{\partial \bar{T}}{\partial \bar{X}} + \frac{\partial \bar{T}}{\partial \bar{Y}}\right) - \frac{\partial \bar{q}_r}{\partial \bar{Y}} + (\rho c)_p D_B \left(\frac{\partial \bar{C}}{\partial \bar{X}}\frac{\partial \bar{T}}{\partial X} + \frac{\partial \bar{C}}{\partial \bar{Y}}\frac{\partial \bar{T}}{\partial \bar{Y}}\right) + (\rho c)_p \frac{D_T}{T_m}\left(\left(\frac{\partial \bar{T}}{\partial \bar{X}}\right)^2 + \left(\frac{\partial \bar{C}}{\partial \bar{Y}}\right)^2\right) + \frac{D_B K_T}{C_s}\left(\frac{\partial^2 \bar{C}}{\partial \bar{X}^2} + \frac{\partial^2 \bar{C}}{\partial \bar{Y}^2}\right), \tag{8}$$

The Nanoparticle concentration equation

$$\left[\frac{\partial \bar{T}}{\partial t} + \bar{U}\frac{\partial \bar{T}}{\partial \bar{X}} + \bar{U}\frac{\partial \bar{T}}{\partial \bar{Y}}\right] = D_B\left(\frac{\partial^2 \bar{C}}{\partial \bar{X}^2} + \frac{\partial^2 \bar{C}}{\partial \bar{Y}^2}\right) + \left(\frac{D_B K_T}{T_m} + \frac{D_T}{T_m}\right)\left(\frac{\partial^2 \bar{T}}{\partial \bar{X}^2} + \frac{\partial^2 \bar{T}}{\partial \bar{Y}^2}\right) - k_1(\bar{C} - \bar{C}_0) \tag{9}$$

Sutterby model components are proposed as, [1], [2], [3], [4], [5]:

$$\bar{\tau}_{\bar{X}\bar{X}} = \frac{\mu}{2}\left[1 - \frac{mD^2}{6}\left\{2\left(\frac{\partial \bar{U}}{\partial \bar{X}}\right)^2 + \left(\frac{\partial \bar{U}}{\partial \bar{X}} + \frac{\partial \bar{U}}{\partial \bar{X}}\right)^2 + 2\left(\frac{\partial \bar{U}}{\partial \bar{X}}\right)^2\right\}\right]2\left(\frac{\partial \bar{U}}{\partial \bar{X}}\right), \tag{10}$$

$$\bar{\tau}_{\bar{X}\bar{Y}} = \frac{\mu}{2}\left[1 - \frac{mD^2}{6}\left\{2\left(\frac{\partial \bar{U}}{\partial \bar{X}}\right)^2 + \left(\frac{\partial \bar{U}}{\partial \bar{X}} + \frac{\partial \bar{U}}{\partial \bar{X}}\right)^2 + 2\left(\frac{\partial \bar{U}}{\partial \bar{X}}\right)^2\right\}\right]2\left(\frac{\partial \bar{U}}{\partial \bar{Y}} + \frac{\partial \bar{U}}{\partial \bar{X}}\right), \tag{11}$$

$$\bar{\tau}_{\bar{Y}\bar{Y}} = \frac{\mu}{2}\left[1 - \frac{mD^2}{6}\left\{2\left(\frac{\partial \bar{U}}{\partial \bar{X}}\right)^2 + \left(\frac{\partial \bar{U}}{\partial \bar{X}} + \frac{\partial \bar{U}}{\partial \bar{X}}\right)^2 + 2\left(\frac{\partial \bar{U}}{\partial \bar{X}}\right)^2\right\}\right]2\left(\frac{\partial \bar{U}}{\partial \bar{Y}}\right), \tag{12}$$

$\bar{R} = (\bar{R}_x, \bar{R}_y, 0)$ is the Darcy components in the axis.

$$\bar{R} = \frac{-\mu}{2k}\left[\frac{sinh^{-1}(D\dot{\xi})}{D\dot{\xi}}\right]^m \bar{V}, \tag{13}$$

The $V(u(x,y,t), v(x,y,t), 0)$velocity, electrical (σ) conductivity material ($\frac{d}{dt}$) time derivative, thermal (K) conductivity, fluid (ρ) density axially-applied electric (E_x) field, pressure (P), extra stress tensor, and Darcy (R) resistance. The wave frame (x, y) is presented as: $x = X - ct, y = Y, u = U - c, v = V, p(x) = P(X,t)$, the non-dimensional quantities $\bar{\psi} = \frac{\psi}{cd}, \bar{X} = \frac{x}{\lambda}, \bar{y} = \frac{y}{d}, \bar{t} = \frac{ct}{\lambda}, \bar{u} = \frac{u}{c}, \bar{v} = \frac{v}{c}, \theta = \frac{\bar{T}_1 - \bar{T}_0}{\bar{T}_0}, \varphi = \frac{\bar{C}_1 - \bar{C}_0}{\bar{C}_0}, \bar{p} = \frac{pd^2}{\mu c\lambda}, k = \frac{R}{d}, \tau_{ij} = \frac{\mu c}{d}\bar{\tau}_{ij}, \Phi = \frac{\bar{\phi}}{\zeta}, u = \frac{\partial \psi}{\partial y}, v = -\delta\frac{\partial \psi}{\partial x}$.

Using the non-dimensional quantities and dropping bars, we will get the following governing model:

$$-\frac{\partial p}{\partial x} + \frac{\partial \tau_{xy}}{\partial y} - M^2\left(\frac{\partial \psi}{\partial y} + 1\right) + G_t\theta + G_c\varphi + \kappa^2 Uhs\,\Phi - \frac{1}{D_a}\left(\frac{\partial \psi}{\partial y}\left[1 - \beta\left(\frac{\partial^2 \psi}{\partial y^2}\right)^2\right]\right) = 0 \tag{14}$$

$$0 = \frac{\partial p}{\partial y}, \tag{15}$$

$$0 = \frac{\partial^2 \theta}{\partial y^2} + B_r\left(\frac{\partial^2 \psi}{\partial y^2}\right)\left[1 - \beta\left(\frac{\partial^2 \psi}{\partial y^2}\right)^2\right] + B_r M^2\left(\frac{\partial \psi}{\partial y} + 1\right)^2 + P_r N_t\left(\frac{\partial \theta}{\partial y}\right)^2 + P_r N_b\left(\frac{\partial \theta}{\partial y}\right)\left(\frac{\partial \varphi}{\partial y}\right), \tag{16}$$

$$0 = N_t\frac{\partial^2 \varphi}{\partial y^2} + N_b\frac{\partial^2 \theta}{\partial y^2} - \eta\,\varphi, \tag{17}$$

$$\tau_{xy} = \left(1 - \beta\left(\frac{\partial^2 \psi}{\partial y^2}\right)^2\right)\frac{\partial^2 \psi}{\partial y^2}. \tag{18}$$

Eliminating the pressure in Eqs. (14), and (15).

$$0 = \frac{\partial^2}{\partial y^2}\left(\left(1 - \beta\left(\frac{\partial^2 \psi}{\partial y^2}\right)^2\right)\frac{\partial^2 \psi}{\partial y^2}\right) - M^2\frac{\partial^2 \psi}{\partial y^2} + \kappa^2 Uhs\frac{\partial \Phi}{\partial y} - \frac{1}{D_a}\frac{\partial}{\partial y}\left(\frac{\partial \psi}{\partial y}\left[1 - \beta\left(\frac{\partial^2 \psi}{\partial y^2}\right)^2\right]\right) + G_t\frac{\partial \theta}{\partial y} + G_c\frac{\partial \varphi}{\partial y}, \tag{19}$$

The Reynolds ($R_e = \frac{\rho_f c d_1}{\mu}$) number, wave ($\delta = \frac{d_1}{\lambda}$) number, Brownian ($N_b = \frac{\tau D_B(\bar{C}_1 - \bar{C}_0)}{\mu}$) motion parameter, Eckert ($E_c = \frac{c^2}{c_f(\bar{T}_1 - \bar{T}_0)}$) number, Prandtl ($P_r = \frac{\mu c_p}{k}$) number, Brinkman ($B_r = E_c P_r$) number, thermophoresis ($N_t = \frac{\tau D_T(\bar{T}_1 - \bar{T}_0)}{\bar{T}_0}$) parameter, chemical ($\eta = \frac{k_1 d_1^2 \rho_f}{\mu}$) reaction parameter, Hartmann ($M = \sqrt{\frac{\sigma}{\mu}}\frac{B_0}{d_1}$) number, local thermal ($G_t = \frac{(1 - C_0)\rho_f g d_1^2 \alpha^*(\bar{T}_1 - \bar{T}_0)}{\mu c}$) Grashof number, local nanoparticle ($G_t = \frac{(\rho_p - \rho_f)g d_1^2 \beta^*(\bar{T}_1 - \bar{T}_0)}{\mu c}$) Grashof number, Sutterby ($\beta = \frac{mB^2 c^2}{6d_1^2}$) fluid parameter, Helmholtz-Smoluchowski ($Uhs = \frac{E_x \varepsilon\zeta}{\mu c}$) velocity, electro-osmotic ($\kappa = dez\sqrt{\frac{2n_0}{\varepsilon k_B T_e}} = \frac{d}{\lambda_d}$) parameter. Using the convenient/appropriate conditions.

$$\psi = \frac{q}{2}, \frac{\partial \psi}{\partial y} = -1, \theta = 0, \varphi = 0 \text{ at } y = h_1(x) = 1 + aCos(2\pi x), \tag{20}$$

$\psi = -\frac{q}{2}, \frac{\partial \psi}{\partial y} = -1, \theta = 1, \varphi = 1$ at $y = h_2(x) =$

$-d - bCos(2\pi x + \phi),$ (21)

The dimensional time mean flow rate Q, in the libratory frame, is related to q through the relation, [24]

$Q = q + 1 + d.$ (22)

3 Analytics and Results

This section is introduced to view the graphical results and presents a numerical comparison table, firstly the verifications of results are offered and then analytics of results are proposed as follows:

3.1 Verifications of Results

To obtain the verifications of numerical results, we put $M = 0, N_b = 0, N_t = 0, G_C = 0$ and $D_a = \infty$, and then compute the results of distributions of velocity and temperature. Finite difference and Generalized-DTM technique are used to get the results of the model offered by, [5], to verify the solutions through Table 1 and found to be good in solution errors 10^{-9}.

3.2 Discussion of Results

A numerical study of the electro-osmotic effects on MHD Sutterby fluid in the presence of generalized Darcy's law is portrayed/computed in this section. Generalized DTM is utilized in computing the graphical results. All graphical results are computed in different two cases, the first of them in the case of dilatant fluid, and the second in the case of non-Newtonian fluid. The fluid distributions are visualized versus a different value of physical parameters of interest through, Figure 2, Figure 3, Figure 4, Figure 5, Figure 6, Figure 7, Figure 8, Figure 9, Figure 10, Figure 11, Figure 12, Figure 13, Figure 14, Figure 15, Figure 16, Figure 17, Figure 18, Figure 19.

The axial $(u(y))$ velocity of the fluid is displayed explicitly against local thermal $((G_t))$ Grashof, electro-osmotic (κ) parameter, Helmholtz-Smoluchowski (Uhs) velocity, Darcy (D_a) number, and Sutterby (β) fluid parameter through Figure 2, Figure 3, Figure 4, Figure 5, Figure 6. Firstly, Figure 2 displays growths in axial $(u(y))$ velocity in the left-hand side, though it declines in the right-hand side for the cases of dilatant and Pseudo-plastic fluids. *Substantially*, the local thermal $((G_t))$ Grashof parameter is definite as the ratio of viscous force and

buoyancy force, a rising in G_t designates a larger buoyancy force. It's depicted in Figure 3, and Figure 4 that a growth in (κ) and (Uhs) declines the axial velocity in the left-hand side while the reverse influences are realized in the right-hand side. *Physically*, the Maximum acceleration of velocity in the region of the walls with rising at the non-variant pressure gradient, whereas, very small acceleration in the center part of the wall is illustrious, accurate, and truthful similar in, [12].

Table 1. Comparisons of velocity and temperature distributions by different mathematical methods at $M = 0, N_b = 0, N_t = 0, G_C = 0$ and $D_a = \infty$.

y	$u(y)$ [5]	$u(y)$ Generalized-DTM	$u(y)$ FDM	$\theta(y)$ [5]	$\theta(y)$ Generalized-DTM	$\theta(y)$ FDM
-1.4	-1	-1	-1	1	1	1
-1.13	-0.525018241	-0.525018763	-0.525018241	1.269730987	1.269730534	1.269730140
-0.859	-0.241212292	-0.241212893	-0.241212292	1.267860254	1.267860645	1.267860243
-0.589	-0.098839088	-0.098839934	-0.098839088	1.123144176	1.123144736	1.123144163
-0.319	-0.058728965	-0.058728893	-0.058728965	0.904607854	0.904607273	0.904607864
-0.049	-0.093684665	-0.093684234	-0.093684665	0.658224309	0.658224984	0.658224308
0.220	-0.186479876	-0.186479873	-0.186479876	0.420374967	0.420374254	0.420374954
0.490	-0.327110576	-0.327110823	-0.327110576	0.220897809	0.220897647	0.220897887
0.760	-0.510525273	-0.510525874	-0.510525273	0.091389918	0.091389547	0.091389974
1.030	-0.734883674	-0.734898303	-0.734883674	0.010940002	0.0109402435	0.010940746
1.3	-1	-1	-1	8.2×10^{-9}	1.7×10^{-8}	2.19×10^{-8}

Afterward (κ) means the ratio of Debye thickness number λ_d to the width of the channel, Uhs influences on velocity $(u(y))$ profile is sketched for common geometries of flow. It is publicized that the axial $(u(y))$ velocity expressively decreases at the left region of the flow channel and its growths in

the right side of the flow channel at high values of Uhs (at $\beta < 0$ & $\beta > 0$). It's seen from Figure 5 that the axial $(u(y))$ velocity neighboring the channel walls is measured as a diminishing function in D_a whilst in the center of the flexible channel opposite behavior is noted in the case of dilatant and Pseudo-plastic fluids (sight effects can be visualized on the right-hand side of the channel more clearly). It's portrayed in Figure 6 that the fluid velocity declines as the pseudoplastic (β) parameter.

Temperature $(\theta(y))$ distribution of fluid is demonstrated graphically against parameters Brinkman (B_r) number, Darcy (D_a) number, thermophoresis (N_t) parameter electro-osmotic (κ) parameter and Helmholtz-Smoluchowski velocity parameter Uhs through Figure 7, Figure 8, Figure 9, Figure 10, Figure 11. It's found in Figure 7 that the temperature distribution has dual phenomena with a raise in B_r that's mean, higher values of B_r advances the fluid temperature near right-wall temporarily rises (B_r) advances heat transfer. Contrariwise near the left wall improves as (B_r) reduces. Growth in D_a causes a growth in the distribution of temperature as seen in Figure 8 (at $\beta < 0$ & $\beta > 0$). Figure 9, Figure 10, Figure 11 displays that the temperature $(\theta(y))$ distribution is a growing function in (N_t), (κ) and (Uhs). *Physically*, increases in κ and Uhs and produce high temperature. κ and Uhs positive value inhibits the thermal diffusion and momentum diffusion whilst κ and Uhs negative value generates thermal diffusion causing an advancement in temperature distribution, exactly and accurately like in, [5].

Concentration $(\varphi(y))$ distribution of fluid is established against Brinkman (B_r) number, Darcy (D_a) number, thermophoresis (N_t) parameter, electro-osmotic (κ) parameter, and Helmholtz-Smoluchowski (Uhs) velocity parameter in Figure 12, Figure 13, Figure 14, Figure 15, Figure 16. It's found from Figure 12 that the nanoparticle $(\varphi(y))$ concentration has a dual phenomenon in case of advance in (B_r). The distribution of nanoparticle concentration decreases with larger values of (B_r) at $y \in [-1.4, -0.02]$, at the same time as the conflicting performance can be imagined at $y \in [-0.01, 1.3]$ Concentration $(\varphi(y))$ distribution is measured as a declining function in (D_a) as publicized in Figure 13. Figure 14, Figure 15 and Figure 16 portrayed that the concentration $(\varphi(y))$ distribution decays in growth in (N_t), (κ) and (Uhs)

accurately and truthful as in, [11]. *Physically*, decreases in (N_t), (κ) and (Uhs) assembly a distinguished decrease in fluid $(\varphi(y))$ concentration while decreasing in velocity leads to significant improvement in Nano-particle $(\varphi(y))$ concentrations. Consequently, the direction of the axial electric field.

Shear stress distribution amplitude of fluid (τ_{xy}) is confirmed graphically against the electro-osmotic (κ) parameter, Darcy (D_a) number, Hartmann (M) number, and Brownian (N_b) motion parameter in Figure 17, Figure 18, Figure 19. Wall shear (τ_{xy}) stress had publicized that the periodic vibrations are similar to the wall geometries owing to the oscillatory nature of the channel walls. Similarly, we have observed that the non-uniform parameters grew as a reduction in wall shear (τ_{xy}) stress oscillatory behavior. It's detected from Figure 17 and Figure 18 that the wall shear stress distribution increases with an increasing magnitude of κ and D_a. In addition, Figure 19 shows that stress tensor increasingly functions in Hartmann number.

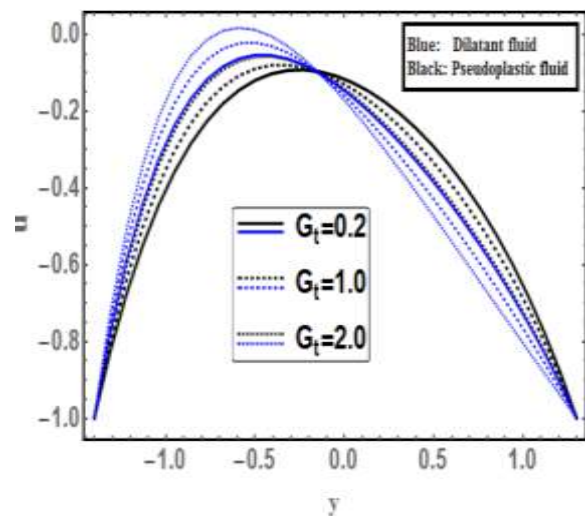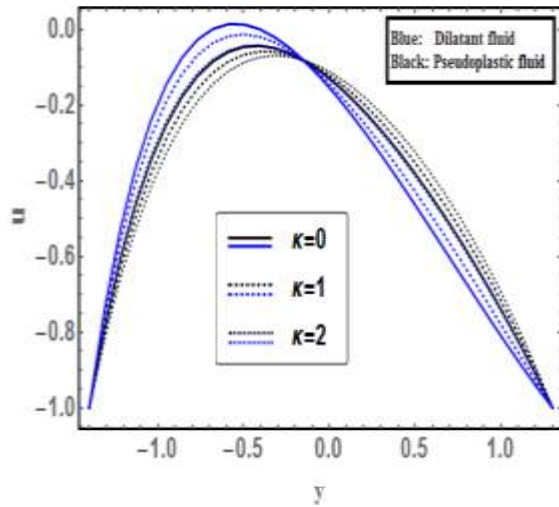
Fig. 2: Velocity $(u(y))$ distribution against G_t.
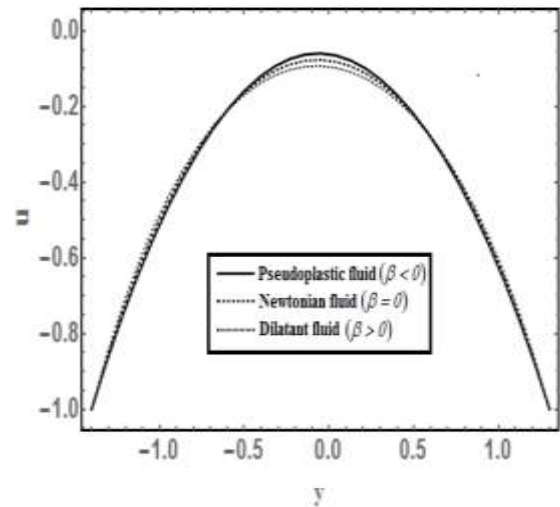
Fig. 3: Velocity (u(y)) distribution against κ

Fig. 4: Velocity (u(y)) distribution against Uhs
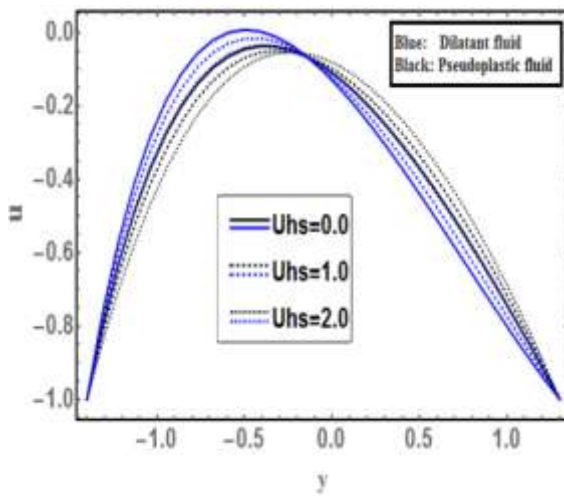

Fig. 5: Velocity (u(y)) distribution against D_a

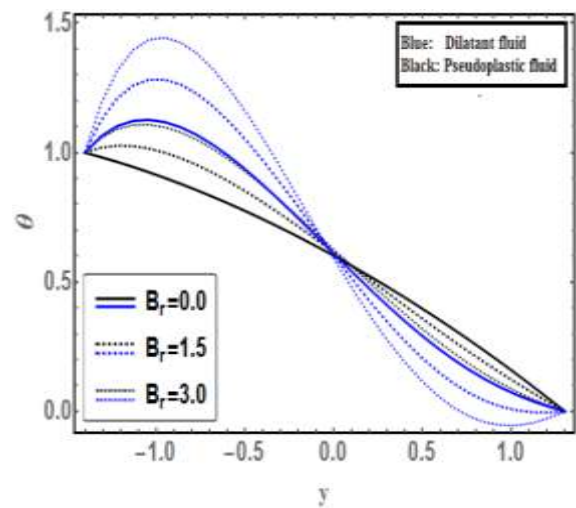

Fig. 6: Velocity (u(y)) distribution against β.
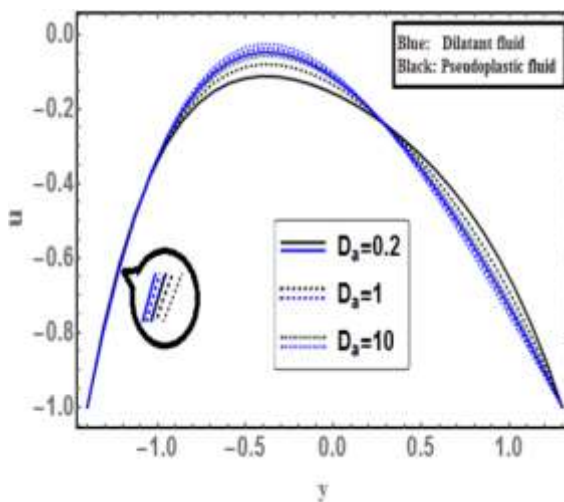
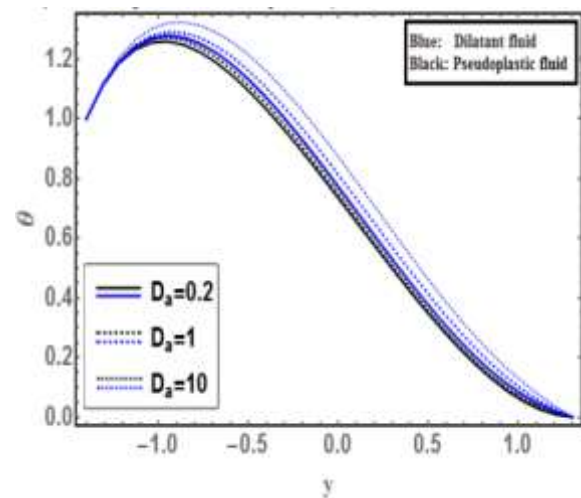

Fig. 7: Temperature (θ(y)) distribution against B_r.

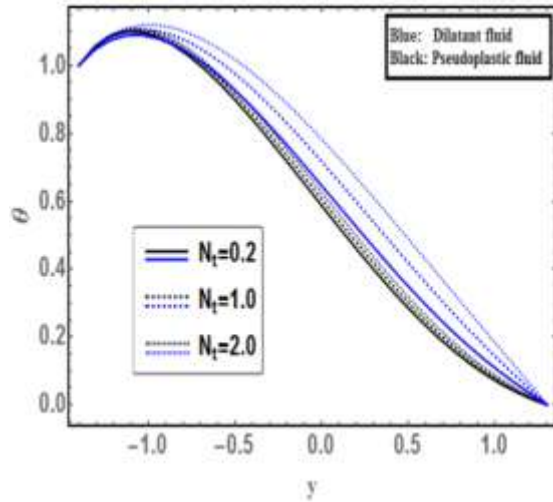Fig. 8: Temperature (θ(y)) distribution against D_a.

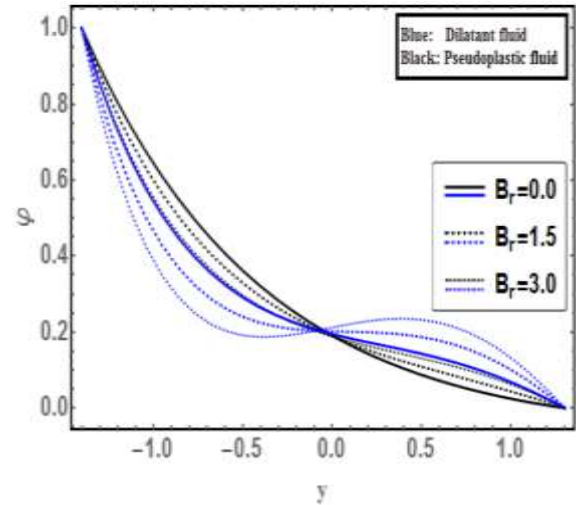Fig. 9: Temperature ($\theta(y)$) distribution against N_t.

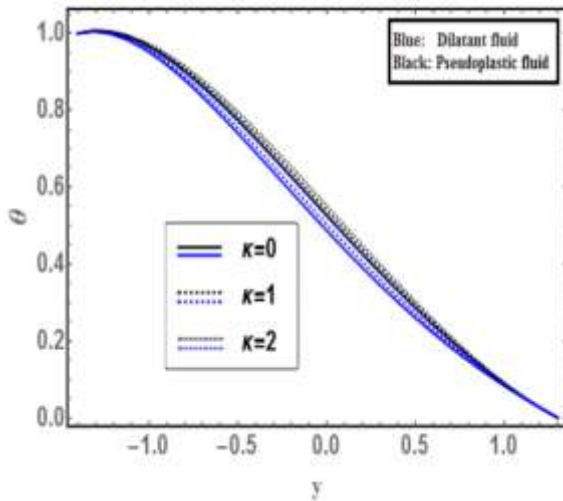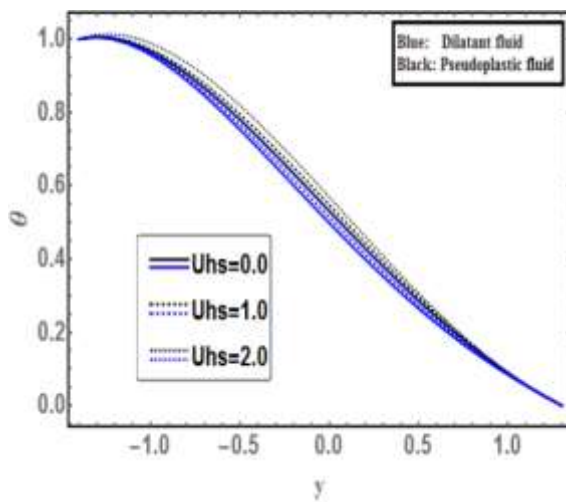Fig. 12: Concentration ($\varphi(y)$) distribution against B_r.

Fig. 10: Temperature ($\theta(y)$) distribution against κ.
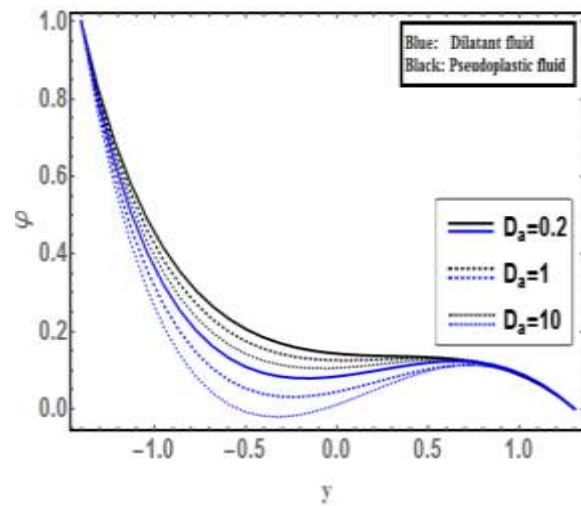
Fig. 13: Concentration ($\varphi(y)$) distribution against D_a.

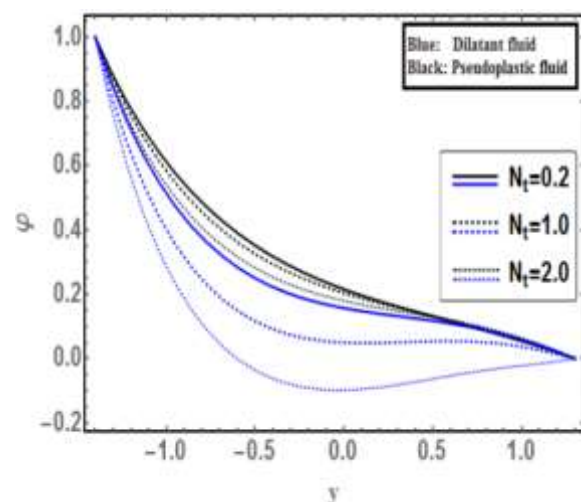Fig. 11: Temperature ($\theta(y)$) distribution against Uhs.

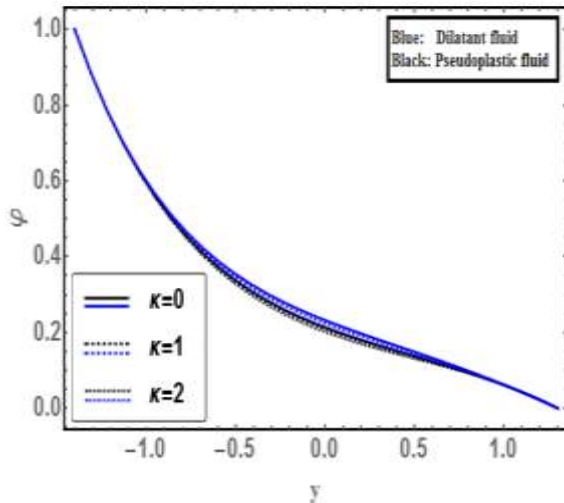Fig. 14: Concentration ($\varphi(y)$) distribution against N_t.

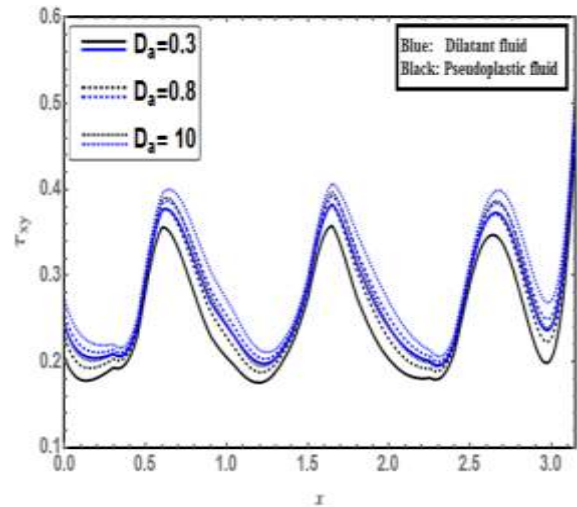Fig. 15: Concentration ($\varphi(y)$) distribution against κ.

Fig. 16: Concentration ($\varphi(y)$) distribution against D_a.

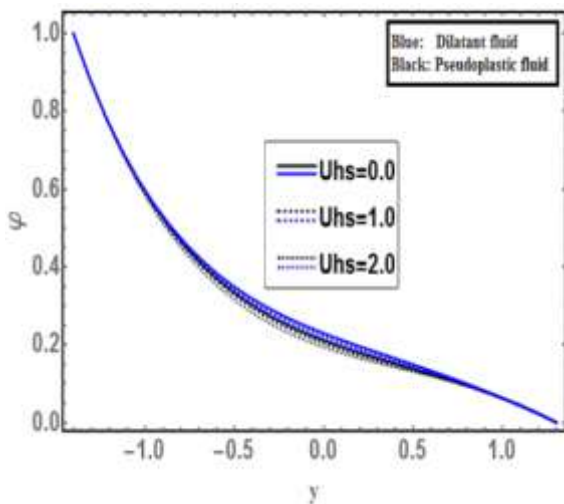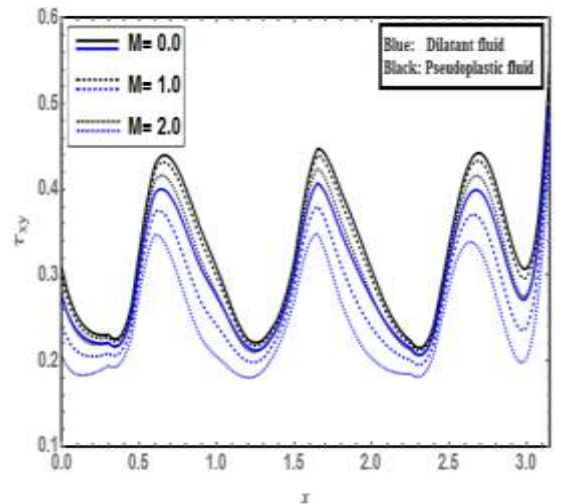Fig. 17: Shear (τ_{xy}) stress profile versus κ.

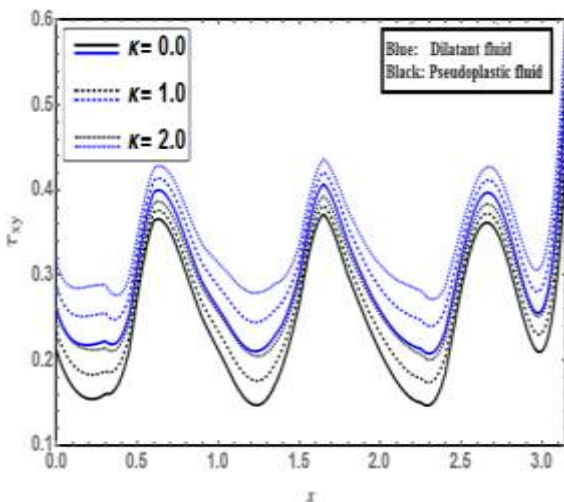Fig. 18: Shear (τ_{xy}) stress profile versus D_a.

Fig. 19: Shear (τ_{xy}) stress profile versus M.

6 Conclusion

Peristaltic pumping of Sutterby fluid in the presence of generalized Darcy's law in an asymmetric channel is deliberated. Results for axial ($u(y)$) velocity, temperature ($\theta(y)$), and concentration($\varphi(y)$) distribution are obtained as a series. The proposed investigation might imply consideration of the blood in cardiovascular system Dynamics. The key results of the presented fluid model are ordered as follows:

- The profile of Shear (τ_{xy}) stress grows in the case of high values of (D_a) and (κ), the influences become more sight in the dilatant fluid than Pseudo-plastic fluid.

- Wall shear (τ_{xy}) stress distribution is considered as a reduction in (M) and (N_b), the behavior

becomes more sight in the dilatant fluid than in Pseudo-plastic fluid.

- A growth in *UHs* tends to an intensification in the temperature profile.
- Sutterby fluid parameter declines ($u(y)$) at the core part of the channel whilst, it increases the velocity distribution at the sides of the channel.
- Brinkman number has a dual role phenomenon on the distributions of temperature and concentration.

References:
[1] J. L. Sutterby, Laminar converging flow of dilute polymer solutions in conical sections: Part I. Viscosity data, new viscosity model, tube flow solution, *AIChE Journal*, Vol. 12, 1966, pp. 63-68.

[2] R. L. Batra and M. Eissa, Laminar forced convection heat transfer of a Sutterby model fluid in an eccentric annulus, *Mechanics Research Communications*, Vol. 21, no. 20, 1994, pp. 147-152.

[3] N. Imran, M. Javed, M. Sohail, P. Thounthong, Z. Abdelmalek, Theoretical exploration of thermal transportation with chemical reactions for Sutterby fluid model obeying peristaltic mechanism, *Journal of Materials Research and Technology*, Vol.9, 2020, pp. 7449–7459.

[4] T. Hayat, S. Ayub, A. Alsaedi, A. Tanveer and B. Ahmad, Numerical simulation for peristaltic activity of Sutterby fluid with modified Darcy's law, *Results in Physics*, Vol. 7, 2017, pp.762–768.

[5] T. Hayat, Hina Zahir, M. Mustafa and A. Alsaedi, Peristaltic flow of Sutterby fluid in a vertical channel with radiative heat transfer and compliant walls: A numerical study, *Results in Physics*, Vol. 6 2016, pp.805– 810.

[6] N. Imran, M. Javed, M. Sohail, P. Thounthong and Z. Abdelmalek, Theoretical exploration of thermal transportation with chemical reactions for sutterby fluid model obeying peristaltic mechanism, *Journal of Materials Research and Technology*, Vol. 9, 2020, pp. 7449–7459.

[7] F. X. Hart and J. R. Palisano, The Application of Electric Fields in Biology and Medicine, *IntechOpen*, (2017).

[8] K. Javid, M. Waqas, Z. Asghar, A. Ghaffari, A theoretical analysis of Biorheological fluid flowing through a complex wavy convergent channel under porosity and electro-magneto-hydrodynamics effects, *Computer Methods and Programs in Biomedicine*, Vol. 191, 2020, 105413.

[9] A. Tanveer, M. Khan, T. Salahuddin and M.Y. Malik, Numerical simulation of electroosmosis regulated peristaltic transport of Bingham Nanofluid, *Computer Methods and Programs in Biomedicine*, Vol. 180, 2019, 105005.

[10] N. K. Ranjit, G. C. Shit, Joule heating effects on electromagnetohydrodynamic flow through a peristaltically induced micro-channel with different zeta potential and wall slip, *Physica A: Statistical Mechanics and its Applications*, Vol. 482, 2017, pp. 458-476.

[11] A, Tanveer, T. Salahuddin, M. Khan, M.Y. Malik, M.S. Alqarni, Theoretical analysis of non-Newtonian blood flow in a microchannel, *Computer Methods and Programs in Biomedicine*, Vol. 191, 2020, 105280.

[12] J. Prakash and D. Tripathi, Electroosmotic flow of Williamson ionic Nanoliquids in a tapered microfluidic channel in presence of thermal radiation and peristalsis, *Journal of Molecular Liquids*, Vol. 256, 2018, pp. 352– 371.

[13] D. Tripathi, Abhilesh Borode, Ravinder Jhorar, O. Anwar Bég, Abhishek Kumar Tiwari, Computer modelling of electro-osmotically augmented three layered microvascular peristaltic blood flow, *Microvascular Research*, Vol. 114, 2017, pp. 65–83.

[14] W. M. Hasona, A.A. El-Shekhipy, M.G. Ibrahim, Combined effects of magnetohydrodynamic and temperature-dependent viscosity on peristaltic flow of Jeffrey nanofluid through a porous medium: Applications to oil refinement, International *Journal of Heat and Mass Transfer*, 126 (2018) 700–714.

[15] A. Bandopadhyay, D. Tripathi, S. Chakraborty, Electroosmosis-modulated peristaltic transport in microfluidic channels,

Physics of Fluids, Vol. 28, No. 5, 2016, 052002.

[16] M. G. Ibrahim, W.M. Hasona and A.A. ElShekhipy, Concentration-dependent viscosity and thermal radiation effects on MHD peristaltic motion of Synovial Nanofluid: Applications to rheumatoid arthritis treatment, *Computer Methods and Programs in Biomedicine*, vol.170, 2019, pp.39–52.

[17] J. Prakash, K. Ramesh, D. Tripathi, R. Kumar, Numerical simulation of heat transfer in blood flow altered by electroosmosis through tapered micro-vessels, *Microvascular Research*, Vol. 118, 2018, pp. 162–172.

[18] W. M. Hasona, N. H. Almalki, A. A. ElShekhipy, M. G. Ibrahim, Thermal radiation and variable electrical conductivity effects on MHD peristaltic motion of Carreau nanofluids: Radiotherapy and thermotherapy of oncology treatment, *Heat Transfer—Asian Res.*, vol.55, 2019, pp.1-19.

[19] X. Wang, J. Wu, Flow behavior of periodical electroosmosis in microchannel for biochips, *Journal of Colloid and Interface Science*, Vol. 293, 2006, pp.483–488.

[20] W. Hasona, N. Al-Malki, A. A. El-Shekhipy, and M. G. Ibrahim, Combined Effects of Thermal Radiation and Magnetohydro-dynamic on Peristaltic Flow of Nanofluids: Applications to Radiotherapy and Thermotherapy of Cancer, *Current NanoScience*, 16(1), (2020) 121-134.

[21] H. Darcy, The Public Fountains of the City of Dijon (Les Fontaines Publiques De La Ville De Dijon). *Dalmont*, Paris, 1856. (p.647 & atlas).

[22] G. R. Machireddy, V. R. Kattamreddy, Impact of velocity slip and Joule heating on MHD peristaltic flow through a porous medium with chemical reaction, J*ournal of the Nigerian Mathematical Society*, Vol. 35, No.1, 2016, pp.227-244

[23] T. Hayat, S. Farooq, B. Ahmad, A. Alsaedi, Effectiveness of entropy generation and energy transfer on peristaltic flow of Jeffery material with Darcy resistance, *International Journal of Heat and Mass Transfer*, Vol. 106, 2017, pp. 244–252.

[24] N. Imran, M. Javed, M. Sohail and I. Tlili, Utilization of modified Darcy's law in peristalsis with a compliant channel: applications to thermal science, *Journal of*

Materials Research and Technology, Vol. 9, 2020, pp.5619–5629.

[25] A. Tanveer, T. Hayat, A. Alsaedi and B. Ahmad, On modified Darcy's law utilization in peristalsis of Sisko fluid, *Journal of Molecular Liquids*, vol.236, 2017, pp.290–297.

[26] J. K. Zhou, Differential Transformation and Its Applications for Electrical Circuits, Huazhong University Press, Wuhan, China, 1986 (in Chinese).

[27] M. G. Ibrahim, N. A. Fawzy, Arrhenius energy effect on the rotating flow of Casson nanofluid with convective conditions and velocity slip effects: Semi-numerical calculations, *Heat Transfer*, Vol. 52, No. 1, 2023, pp. 687-706

[28] M. G. Ibrahim, Adaptive Computations to Pressure Profile for Creeping Flow of a Non-Newtonian Fluid with Fluid Nonconstant Density Effects, *J. Heat Transfer*, Vol. 144, No. 10, 2022, 103601.

[29] M. G. Ibrahim, Adaptive simulations to pressure distribution for creeping motion of Carreau nanofluid with variable fluid density effects: *Physiological applications, Thermal Science and Engineering Progress*, Vol. 32, No. 1 2022, 101337.

[30] M. G. Ibrahim, Numerical simulation for non-constant parameters effects on blood flow of Carreau–Yasuda nanofluid flooded in gyrotactic microorganisms: DTM-Pade application, *Archive of Applied Mechanics*, Vol. 92, 2022, pp.1643–1654.

[31] M. G. Ibrahim, Concentration-dependent viscosity effect on magnet nano peristaltic flow of Powell-Eyring fluid in a divergent-convergent channel, *International Communications in Heat and Mass Transfer*, Vol. 134, 2022, 105987.

[32] M. G. Ibrahim, Numerical simulation to the activation energy study on blood flow of seminal nanofluid with mixed convection effects, *Computer Methods in Biomechanics and Biomedical Engineering*, 2022, 2063018.

[33] M. G. Ibrahim, Naglaa Abdallah, and Mohamed Abouzeid, Activation energy and chemical reaction effects on MHD Bingham nanofluid flow through a non-Darcy porous media, *Egyptian Journal of Chemistry*, 2022.117814.5310.

[34] M. G. Ibrahim and Hanaa A. Asfour, The effect of computational processing of

temperature- and concentration-dependent parameters on non-Newtonian fluid MHD: Applications of numerical methods, Heat Transfer, Vol. 55, 2022, pp. 1-18.

[35] M. G. Ibrahim, W. M. Hasona and A. A. ElShekhipy, Instantaneous influences of thermal radiation and magnetic field on peristaltic transport of Jeffrey nanofluids in a tapered asymmetric channel: *Radiotherapy of oncology treatment, Advances, and Applications in Fluid Mechanics*, Vol. 24, No. 2, 2021, pp. 25-55.

Contribution of Individual Authors to the Creation of a Scientific Article (Ghostwriting Policy)
The authors equally contributed in the present research, at all stages from the formulation of the problem to the final findings and solution.

Conflict of Interest
The authors have no conflict of interest to declare.